small
NANO MICRO

Conjugated Polymer/Nanocrystal Nanocomposites for Renewable Energy Applications in Photovoltaics and Photocatalysis

*Yu-Wei Su, Wei-Hao Lin, Yung-Jung Hsu, and Kung-Hwa Wei**

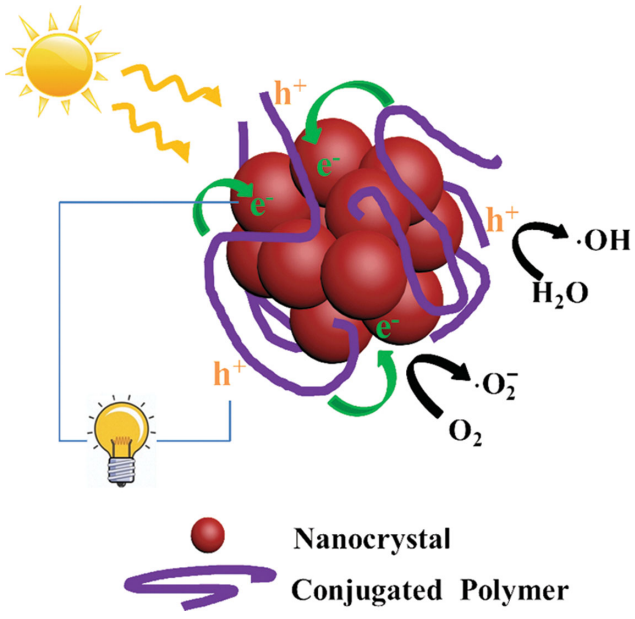

From the Contents

Conjugated polymer/nanocrystal composites have attracted much attention for use in renewable energy applications because of their versatile and synergistic optical and electronic properties. Upon absorbing photons, charge separation occurs in the nanocrystals, generating electrons and holes for photocurrent flow or reduction/oxidation (redox) reactions under proper conditions. Incorporating these nanocrystals into conjugated polymers can complement the visible light absorption range of the polymers for photovoltaics applications or allow the polymers to sensitize or immobilize the nanocrystals for photocatalysis. Here, the current developments of conjugated polymer/nanocrystal nanocomposites for bulk heterojunction–type photovoltaics incorporating Cd- and Pb-based nanocrystals or quantum dots are reviewed. The effects of manipulating the organic ligands and the concentration of the nanocrystal precursor, critical factors that affect the shape and aggregation of the nanocrystals, are also discussed. In the conclusion, the mechanisms through which conjugated polymers can sensitize semiconductor nanocrystals (TiO_2, ZnO) to ensure efficient charge separation, as well as how they can support immobilized nanocrystals for use in photocatalysis, are addressed.

1. Introduction

Semiconductor nanocrystals exhibiting quantum confinement properties, so-called "quantum dots" (QDs), are emerging as functional materials for applications in light harvesting and photocatalysis because of their size-tunable band gaps and large surface-to-volume ratios that allow them to interact with other materials (e.g., polymers). In order to produce size-tunable band gaps, the size range of nanocrystal QDs must be comparable to or smaller than the Bohr exciton radius—the size of exciton (a pair of bonded electron and hole) in bulk semiconductors. This feature of nanocrystal QDs restricts carrier (electrons and holes) motion in all three spatial dimensions. As the size decreases, the electronic excitations shift to higher energy and results in a higher band gap energy (E_g). Upon absorbing light, an electron is excited from the valence band to the conduction band of the QD; when these QDs form heterojunctions with off-set energy band structures with conjugated polymers, the excitons can readily dissociate into free charge carriers. These photo-induced and dissociated charge carriers can then migrate to their respective electrodes (allowing photovoltaics applications) or diffuse to the nanocrystal surface to mediate reduction/oxidation (redox) reactions (allowing photocatalytic applications). Incorporating nanocrystals into conjugated polymers can not only facilitate photovoltaics device fabrication on flexible substrates and the use of wet-processing techniques (e.g., roll-to-roll coating or printing)[1] but also provide the possibility to have a large interfacial area for efficient exciton dissociation.[2] In this Article, we review the conjugated polymer/nanocrystals composites that have been used for photovoltaics and photocatalysis applications.

Traditional silicon and thin film photovoltaics harvest only approximately 33% of the energy from any given solar photons; another 33% is lost to thermalization, with the remaining 34% being energy that is not absorbed or unavoidable thermodynamic losses.[3] The use of nanocrystal QDs in photovoltaics can lead to a higher limiting conversion efficiency through either recovery of some energy lost through thermalization or providing pathways to harvest those photons not absorbed in a tradition solar cell.[4] Chalcogenide (PbX, CdX; X = S, Se, Te) nanocrystal QDs have attracted attention for use in solar cells because of the potential for multiple exciton generation (MEG), also known as the impact ionization process.[5–7] In the impact ionization process, a high-energy exciton, created by absorbing a photon of energy that is much larger than the band gap of the QDs ($\geq 2E_g$), relaxes to the band edge and transfers energy to another electron in the valence band to overcome the band gap energy required to transfer its excited electron to the conduction band; therefore, this process has the potential to generate more than one electron/hole pair after the absorption of a single photon, thereby increasing the photocurrent, and thus, the power conversion efficiency (PCE) of the photovoltaic device. The effect of MEG of the QDs on conjugated polymer/QDs nanocomposite was found to be able to enhance external quantum efficiency (EQE) up to 150% at negative biases,[8] but no other studies on this phenomenon has been reported. For conjugated polymers to be used in organic photovoltaics, they should ideally possess i) low band gaps, to broaden the absorption range; ii) crystalline characteristics, to ensure good charge mobility; and iii) suitably low energy levels for their highest occupied molecular orbitals (HOMOs), to enhance the open-circuit voltages (V_{oc}) of their devices. In reality, polymers having low band gaps generally require large conjugated structures, which sometimes are difficult to synthesize and to dissolve, and they often are not capable of efficiently converting absorbed photons, from the infrared region, into electrons. These problems can be overcome by incorporating QDs possessing tunable band gaps, allowing light absorption by these QDs to complement that of the conjugated polymers, resulting in nanocomposites that can extend the absorption range further into the infrared region. Many reports have appeared regarding the development of ligands to improve the dispersion and electronic structure of nanocrystal QDs,[9] the construction of polymer/nanocrystal nanocomposite solar cells,[3,10–14] and the analysis of charge transfer (CT) kinetics.[15]

Photocatalysis is a green technique that has been applied widely in the fields of environmental remediation, antibacterial treatment, selective organic transformations, and solar water splitting. To effectively drive desired redox reactions mediated by photoinduced charge carriers, a semiconductor nanocrystal must have a suitable band gap energy with appropriate energy levels for their conduction bands (analogous to the lowest unoccupied molecular orbital (LUMO) in an organic molecule) and valence band (analogous to the highest occupied molecular orbital (HOMO)). Overall, water splitting requires the bottom level of the conduction band to be more negative than the redox potential of H^+/H_2 (0 V vs NHE), while the top level of the valence band should be more positive than the redox potential of H_2O/O_2 (1.23 V vs NHE).[16] Thus, the minimum value of E_g of a semiconductor nanocrystal for water splitting should be 1.23 eV, but preferably greater than 2.0 eV in a practical setting to overcome energy losses caused by the kinetic overpotentials. Several issues in semiconductor nanocrystal photocatalysis remain unsolved: i) the photocatalytic efficiency of semiconductor nanocrystals is commonly suppressed by the inherently fast recombination of charge carriers; ii) most semiconductor photocatalysts currently available (e.g., TiO_2, ZnO) can function in the UV or near-UV region, and some approaches have been adopted to impart them with visible absorption, for instance the utilization of plasmonic effect from gold nanocrystal on TiO_2; [17–19] iii) most semiconductor photocatalysts are prepared in powder form and are prone to forming aggregates during photocatalysis processes. In recent years, nanocomposite photocatalysts comprising semiconductor nanocrystals and conducting polymers have demonstrated remarkable photocatalytic properties, promoting effective charge separation to increase the

Dr. Y.-W. Su, W.-H. Lin, Prof. Y.-J. Hsu, Prof. K.-H. Wei
Department of Materials Science and Engineering
National Chiao Tung University
Hsinchu 30010, Taiwan
E-mail: khwei@mail.nctu.edu.tw

DOI: 10.1002/smll.201401508

NANO MICRO small

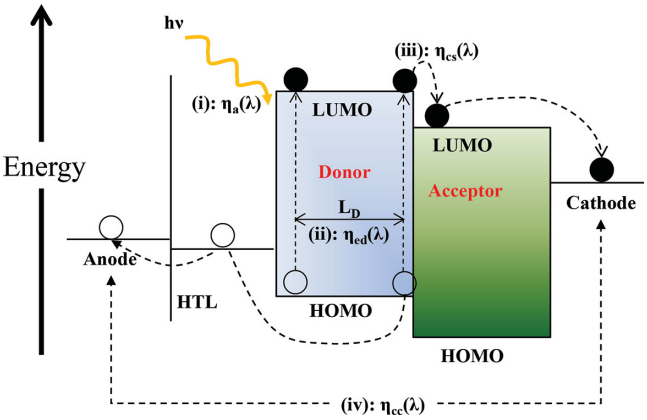

Figure 1. Fundamental mechanism of the photon-to-electron conversion process in BHJ solar cells. Reproduced with permission.[24] Copyright 2012, Elsevier Ltd.

carrier utilization efficiency along with simple removal from reaction solutions. Their conducting polymers serve as photosensitizers for the semiconductor nanocrystals, allowing them to produce additional charge carriers and improve the photocatalytic performance; in addition, the polymers serve as host materials that immobilize the semiconductor nanocrystals, thereby improving the stability of the photocatalysts and maintaining the photocatalytic activity.[20–22]

2. Photovoltaics Application

Figure 1 presents the energy diagram of a bulk heterojunction (BHJ) solar cell. The photon-to-electron conversion mechanism involves four fundamental steps. In the first step, the absorption of light causes photoinduced excitation of an electron in the donor from the HOMO to the LUMO, forming a Frenkel exciton [i.e., a coulombically bound electron (e^-) and hole (h^+)]. The excitons in organic materials have binding energies in the range from 0.5 to 1 eV; [23] because these values are much higher than thermal energy (kT = 0.025 eV) at room temperature (298 K), a second material—an electron acceptor—must be present to ensure a built-in internal field at the interface, thereby dissociating any excitons into their free carriers. Nanocrystals (n-type materials) can, for example, be used as acceptor materials to replace the fullerene units while polymers remain as the donor materials in polymer/fullerene–based solar cells[24,25] to form donor–acceptor (D–A) interfaces. In the second step, the excitons diffuse to the D–A interfaces within the diffusion length to prevent recombination for releasing photon energy and returning to the ground state. In the third step, an exciton at a D–A interface undergoes ultra-rapid CT to form a CT exciton with the hole and electron remaining in the D and A phases, respectively, held together through coulombic attraction. In the fourth step, the built-in electric field causes the CT excitons to dissociate into free holes and electrons, which then travel through the D and A phases to their respective electrodes. These four steps in the photon-to-electron conversion process are characterized by four conversion efficiencies: the absorption efficiency (η_A), the exciton diffusion efficiency (η_{ED}), the charge separation efficiency (η_{CS}), and the charge collection efficiency (η_{CC}), respectively. The EQE is defined, in terms of energy, as the ratio between the number of collected photogenerated charges at the electrodes and the number of incident of photons at a particular wavelength (λ); it can be expressed as

$$EQE(\lambda) = \eta_A(\lambda) \times \eta_{ED}(\lambda) \times \eta_{CS}(\lambda) \times \eta_{CC}(\lambda) \quad (1)$$

The PCE (%), of a photovoltaic device is defined as

$$PCE = (J_{sc} \times V_{oc} \times FF) / (P_{in}) \quad (2)$$

where J_{sc} is the short-circuit current density, V_{oc} is the open-circuit voltage, FF is the fill factor, and P_{in} is the power of the incident light. Equation (3) can be used to provide a theoretical value of J_{sc} for comparison with the value obtained experimentally from the current density–voltage (J–V) measurements:

Yu-Wei Su received his M.S. and Ph.D. degrees from the School of Chemical, Biological & Environmental Engineering, Oregon Strate University in 2007 and 2011, respectively. He joined Prof. Kung-Hwa Wei's group in National Chiao Tung University as a postdoctoral fellow since 2012. His research interests include inorganic, organic photovoltaics and using small angle X-ray scattering for polymer structure.

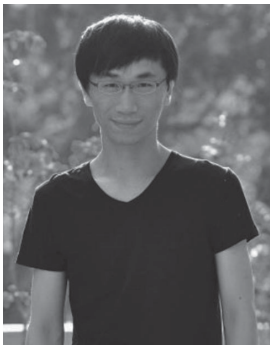

Yung-Jung Hsu is an Associate Professor in the Department of Materials Science and Engineering, National Chiao Tung University, Taiwan. He received his Ph.D. degree in Chemical Engineering from National Tsing Hua University, Taiwan, in 2005. After his postdoctoral fellow working at National Tsing Hua University, he joined National Chiao Tung University and started the independent research career in 2007. His research interests include preparation of semiconductor nanoheterostructures, investigation of interfacial charge carrier dynamics, and development of advanced nanomaterials for photoconversion applications.

Kung-Hwa Wei is a distinguished Professor in the Department of Materials Science and Engineering, National Chiao Tung University, Taiwan. He received his Ph.D. degree in Chemical Engineering from University of Massachusetts, Amherst, in 1987, and then worked at Wright-Patterson Air Force base and General Electric company before joining the University in 1993. His research interests include conjugated polymers, colloidal quantum dots and metal nanoparticles nanocomposites, and graphene for photovoltaics, bio-sensing, electronic, and nonvolatile memory applications.

$$J_{sc} = \frac{hc}{q}\int \frac{P_{sun}(\lambda)EQE(\lambda)}{\lambda}d\lambda \quad (3)$$

where $P_{sun}(\lambda)$ represents the power of photons at each wavelength of the solar spectrum. q is the elementary charge, h is Planck's constant, and c is the speed of light.

When inorganic nanocrystals are used as electron acceptors in a BHJ solar cell, they must have an electron affinity higher than that of the donor polymers to ensure efficient exciton dissociation and CT at the interfaces. Replacing the fullerene units with nanocrystals should have several benefits:[14] i) the light absorption contribution of chalcogenide QDs is greater than that of fullerene derivatives, leading to enhanced photogeneration of charge carriers; ii) the light absorption of nanocrystals can be tuned to cover a broad spectral range through modifications of the sizes and shapes; iii) nanocrystals provide ultrafast and efficient photoinduced charge carrier transfer between D and A materials; iv) nanocrystals have relatively high electron mobilities and good photostability and chemical stability. Despite all these benefits, the capping ligands on the QDs play an important role in their interface properties that determine the extent of mixing with the conjugated polymers as well as the carrier transport in these nanocomposites.

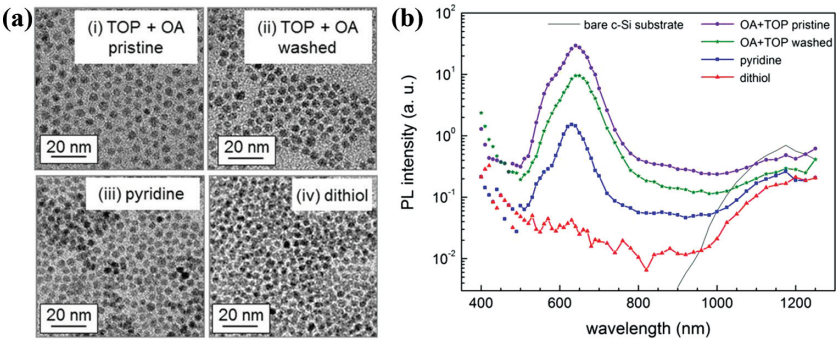

Figure 3. a) TEM images and b) PL measurement of CdSe QDs presenting various surfactants. Reproduced with permission.[29] Copyright 2012, American Chemical Society.

2.1. Preparation and Morphology of Polymer/Nanocrystal QDs

Colloidal CdSe QDs are typically synthesized through thermal decomposition (280–300 °C) of an organometallic Cd precursor with a Se precursor in a hot solution of hexylphosphonic acid, trioctylphosphine oxide (TOPO), tributyl- or trioctylphosphine (TOP), or hexadecylamine (HDA). When the reaction is complete, the solution is suddenly cooled to room temperature to quench any further nucleation; it is then added into methanol to precipitate the nanocrystal CdSe QDs. After washing to remove any excess capping ligands, monodisperse nanocrystal QDs are obtained; their size and shape can be controlled by the reaction time and the ratio of surfactants, injection volume and the monomer concentration, respectively.[26,27] **Figure 2** displays the photoluminescence (PL) spectra of CdSe nanocrystals synthesized in TOPO and in a TOPO/HDA mixture. Upon increasing the reaction time, pure TOPO as solvent resulted in a nearly linear increase in the emission line widths, whereas the mixed solvent led to constant emission line widths.[28]

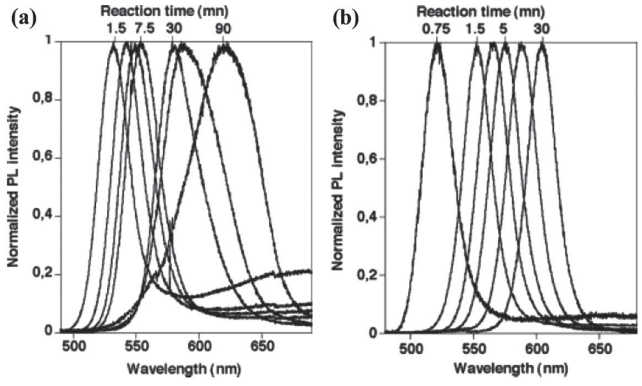

Figure 2. Evolution of the PL spectra during the synthesis of CdSe nanocrystals in a) TOPO and b) TOPO/HDA (molar ratio: 1:4). Reproduced with permission.[28] Copyright 2002, American Chemical Society.

Figure 3a displays transmission electron microscopy (TEM) images of CdSe QDs stabilized with TOP and oleic acid (OA) (both pristine and washed), pyridine, and dithiol molecules. The pristine TOP/OA–capped QDs exhibited a regular hexagonal arrangement with the largest averaged interparticle distance of 7.7 nm between the QD centers. An additional ligand exchange process with 1,4-benzenedithiol (dithiol) decreased the distance to 5.5 nm. Figure 3b presents PL spectra for the CdSe QDs coated with TOP and OA (both pristine and washed), pyridine, and dithiol molecules. The relative intensity of the first excitonic peak at 640 nm followed the sequence pristine > washed > pyridine-coated QDs; this peak was not observable for the dithiol-coated QDs. Pyridine ligand exchange provided an even higher number of trap states, enabling a decrease in radiative recombination as a result of the stabilized electrons in the π rings of the pyridine units. Exchange with dithiol decreased the PL signal intensity to almost zero, indicating that quenched radiative recombination arose from trapped holes in the lone pairs of sulfur atoms, which forms covalent bonds with cadmium atoms.[29]

Figure 4 presents TEM images of blends of poly(2-methoxy,5-(2-ethyl)-hexyloxy-*p*-phenylenevinylene) (MEH-PPV) with pyridine-treated CdSe or TOPO-coated CdSe, with various weight percentages of the nanocrystals. The pyridine-treated CdSe nanocrystals aggregated together to form regions of densely packed nanocrystals surrounded by regions of polymer. As the concentration of nanocrystals increased, more nanocrystals aggregated to form a larger domain and a connected network in the plane of the film. In contrast, the TOPO-coated CdSe nanocrystals underwent almost no aggregation at low concentration, because TOPO and MEH-PPV both have nonpolar faces. This morphology provides a rationale for why, in subsequent studies, solar cells required a sufficiently high weight percentage of nanocrystals (>80%) to ensure efficient quenching of the PL.[30]

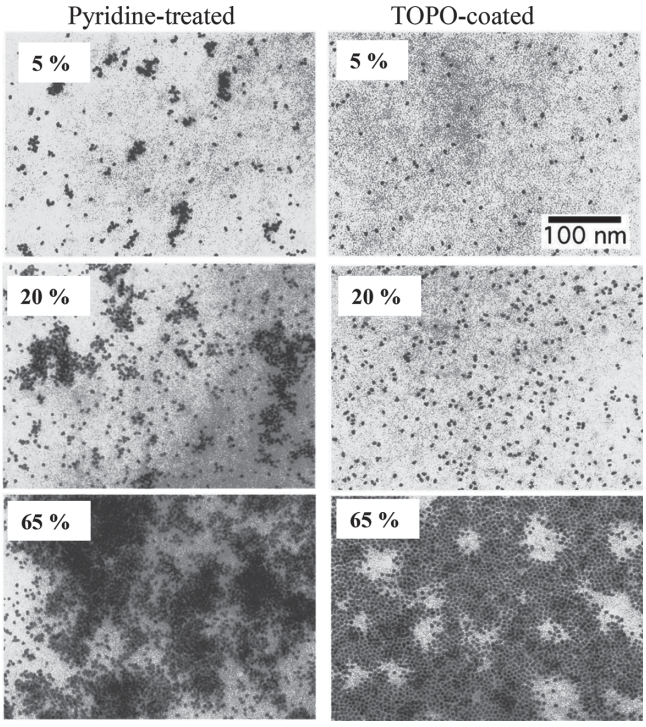

Figure 4. TEM images of blends of MEH-PPV with pyridine-treated CdSe and TOPO-coated CdSe at nanocrystal concentrations of 5, 20, and 65% (w/w). Reproduce with permission.[30] Copyright 1996, American Physical Society.

In 1992, fullerene (C_{60} or C_{70})-doped polymers were reported to exhibit photoconductivity;[31] subsequent studies revealed that photocurrents could be achieved when using semiconductor nanocrystals to photosensitize needlelike C_{60} crystals.[32] A cluster shell comprising CdSe QDs surrounded by functionalized C_{60} molecules exhibited a superior photocurrent response, with ultrafast electron transfer between the CdSe QD and the functionalized fullerene.[33,34] An alternative method was developed for the in situ generation of CdSe QDs in a polymer nanocomposite film through thermal decomposition of a complex cadmium precursor blended with the polymer.[35]

2.2. Cadmium-Based Nanocrystals

Figure 5 presents the chemical structures of some representative polymers that have been applied in the solar cells based on polymer/nanocrystal nanocomposites that are discussed in this Review. Poly-(3-hexylthiophene) (P3HT) as an electron-donor material has been attractive for forming P3HT/CdX (X = S, Se) BHJ solar cells because it allows effective hole transport in its regioregular form. **Table 1** lists all reported device characterization data for nanocomposite solar cells incorporating polymer/Cd-based nanocrystal blends. The size and concentration of the CdSe nanorods in the P3HT/CdSe blend solution can be tuned to control the degree of nanocrystal aggregation and to obtain high EQEs (>54%) and PCEs (ca. 2%).[36,37] In addition, the incorporation of three-dimensional hyperbranched CdSe nanocrystals into solution blends produces an active layer having large and distributed surface area for charge separation.[38] Other parameters, including the nature of the solvent,[39] the annealing temperature, the annealing time,[40] the nanocrystal size,[41] and the nature of the ligand on CdSe,[42,43] have also been studied intensively to optimize the device fabrication process. A modified device architecture featuring ZnO nanoparticles as a buffer layer between the active layer (P3HT/CdSe) and the metal electrode (Al) has been demonstrated that the stability of the device enhanced to 60–70% of the original PCE after exposed to ambient condition for 70 days, as compared to a few hours life time without the ZnO layer.[44]

Recently, a chemical grafting approach was developed to bind CdS QDs onto P3HT nanowires,[45] allowing control over organic/inorganic phase separation and significantly improving the PCE to 4.1% from 0.6% for the approach without chemical grafting. A post-treatment process—immersing the substrate with the polymer/CdSe blend film into an acetonitrile solution containing 1% ethanedithiol (EDT)—was used to remove the charged phosphonic acid ligands from the surfaces of the CdSe nanorods and form monolayer-passivated

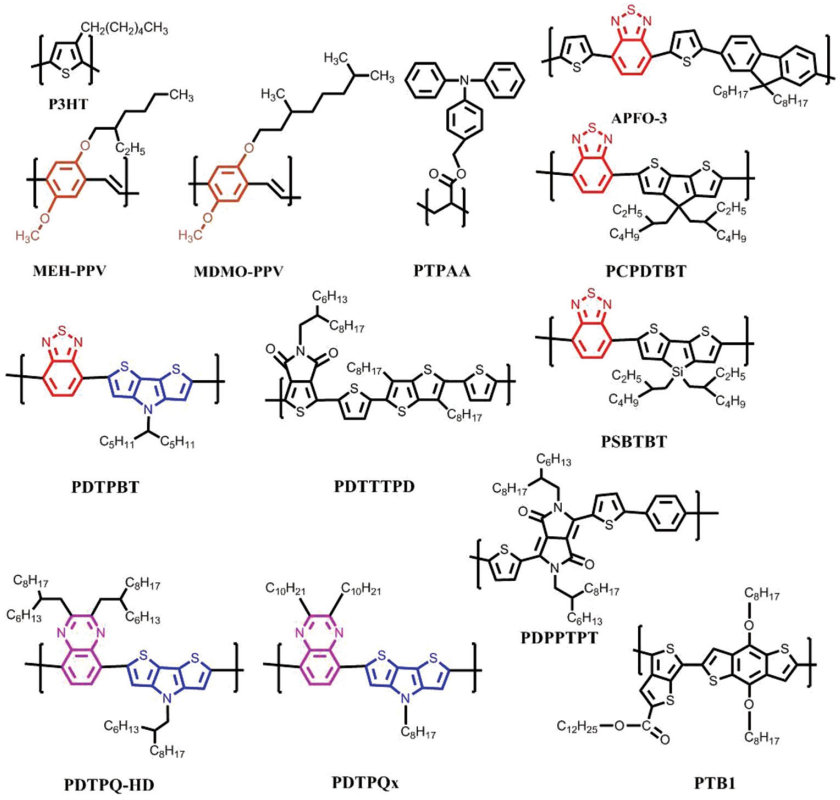

Figure 5. Chemical structures of representative polymers that have been incorporated in the solar cells based on polymer/nanocrystal nanocomposites that are discussed in this Review.

Table 1. Device characterization data for nanocomposite solar cells incorporating polymer/Cd–based QD blends.

Ref.	Polymer	QD	V_{oc} [V]	J_{SC} [mA cm^{-2}]	FF	PCE [%]
Huynh[37]	P3HT	CdSe	0.70	5.7	0.40	1.7
Sun[a)][39]	P3HT	CdSe	0.62	8.79	0.50	2.6
Olson[40]	P3HT	CdSe	0.55	6.87	0.47	1.8
Zhou[42]	P3HT	CdSe	0.62	5.80	0.56	2.0
Yang[41]	P3HT	CdSe	0.70	6.50	0.40	1.9
Qian[44]	P3HT	CdSe	0.64	6.30	0.54	2.2
Ren[45]	P3HT	CdS	1.10	10.9	0.35	4.1
Albero[43]	P3HT	CdS	0.55	5.61	0.66	2.0
Zhou[46]	P3HT	CdSe	0.73	7.40	0.54	2.9
Greeham[b)][30]	MEH-PPV	CdSe	0.50	0.014	0.26	0.2
Sun[c)][50]	MDMO-PPV	CdSe	0.76	6.42	0.44	2.4
Böhm[52]	MDMO-PPV	CdSe	0.72	5.7	N/A	1.7
Snaith[d)][51]	PTPAA	CdSe	0.85	N/A	N/A	N/A
Wang[54]	APFO-3	CdSe	0.95	7.23	0.35	2.4
Dayal[55]	PCPDTBT	CdSe	0.67	9.02	0.51	3.1
Albero[57]	PCPDTBT	CdSe	0.61	6.89	0.28	1.2
Zhou[56]	PCPDTBT	CdSe	0.78	9.20	0.49	3.7
Kuo[59]	PDTTTPD	CdSe	0.88	7.26	0.46	2.9

[a–c)]Incident power: a) 92, b) 0.5, and c) 90 mW cm^{-2}; [d)]Illumination conditions: monochromic light; wavelength: 400 nm.

Cd-thiolate nanorods. Such EDT treatment decreased exciton and charge carrier recombination and increased charge transport in the polymer/CdSe hybrid film, resulting in an increase in PCE to 2.9% from 2.2%.[46] A comparative study indicated that a major fraction of the successfully separated charge carriers in the P3HT/CdSe blends were trapped in deep localized states, whereas the geminate recombination resulted from only shallow traps in P3HT/fullerene blends.[47]

Low band gap conjugated polymers have also been studied for organic/inorganic hybrid photovoltaic applications. Before P3HT was used as an electron-donor material, MEH-PPV[30] had been blended with CdSe and CdS nanocrystals for use in solar cell devices. The absorption intensity in the visible light range (600–650 nm) increases with the weight percentage of CdSe in MEH-PPV/CdSe blends; the PCE reached to 0.2% under AM 1.5 conditions at an incident energy of 0.5 mW cm^{-2} when 90 wt% CdSe was incorporated. **Figure 6** presents three possible routes for exciton separation and CT in MEH-PPV/CdSe blends. Excitons created in MEH-PPV can experience charge separation through electrons transferring from the polymer to the nanocrystal (route a). Alternatively, if the exciton is created on the nanocrystal (route c), or transfers onto the nanocrystal (route b), the hole can subsequently transfer to the polymer, producing a separated state of an electron on the nanocrystal. If CdSe nanocrystals are replaced by CdS nanocrystals, the excitons generated in the polymer are unable to transfer to the nanocrystals, because the band gap of CdS is larger than that of the polymer.[30] Photoinduced absorption spectroscopy has been used to observe long-lived positive polarons in MEH-PPV/CdSe blends following electron transfer to the nanocrystals.[48] Many subsequent studies have focused on using polymer/CdSe nanocrystal systems to keep improving device performance. Polymer derivatives featuring modified side chains, including poly(2-methoxy-5-(3′,7′-dimethyloctyloxy)-*p*-phenylenevinylene) (MDMO-PPV)[49,50] and poly(triphenylamine acrylate) (PTPAA)[51] can improve

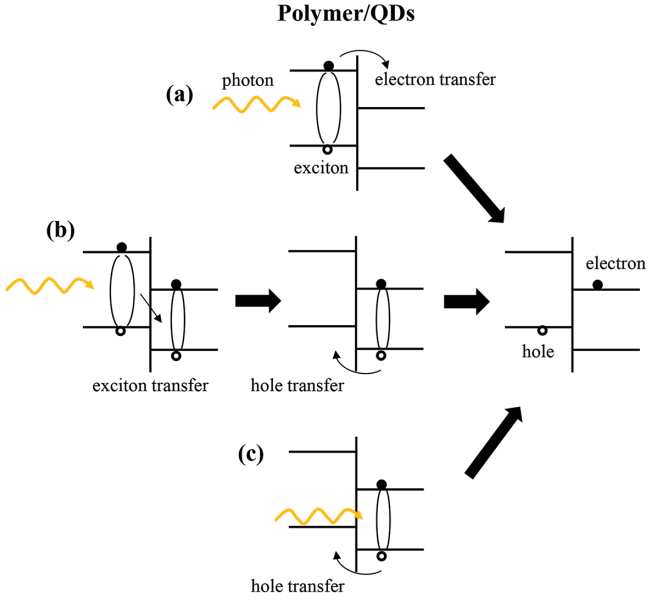

Figure 6. Routes for exciton transfer and CT in MEH-PPV/CdSe blends. a) Exciton created in the polymer after absorption, followed by electron transfer onto the nanocrystal. b) Exciton created in the polymer after absorption, followed by exciton transfer onto the nanocrystal, followed by hole transfer onto the polymer. c) Exciton created in the polymer after absorption in the nanocrystal, followed by hole transfer onto the polymer. Reproduced with permission.[30] Copyright 1996, American Physical Society.

small NANO MICRO

Table 2. Device characterization data for nanocomposite solar cells incorporating polymer/Pb–based QD blends.

Refs.	Polymer	QD	V_{oc} [V]	J_{SC} [mA cm^{-2}]	FF	PCE [%]
Watt[a)][61]	MEH-PPV	PbS	1	0.13	0.28	0.7
Noon[62]	PDTPQx	PbS	0.38	4.20	0.34	0.6
Seo[63]	PDTPBT	PbS	0.57	13.06	0.51	3.8
Piliego[66]	PDPPTPT	PbS	0.47	12.5	0.49	2.9
Nam[70]	PSBTBT	PbS	0.63	10.82	0.51	3.5
Nagaoka[71]	PTB1	PbS	0.49	15.8	0.36	2.8
Zhang[b)][73]	PCPDTTBTT	PbS	0.63	12.99	0.52	4.2
Cui[75]	P3HT	PbSe	0.35	1.08	0.37	0.1
Jiang[76]	P3HT	PbSe	0.32	0.24	0.43	0.04

[a)]Incident power: 5 mW cm^{-2}; [b)]Planar structure device.

the PCE to over 2%. Treatment of *n*-butylamine–capped CdSe with hexane could expel aggregated and poorly passivated CdSe nanocrystals, thereby resulting in a finer morphology and better long-range connectivity of the nanocrystal network.[52] Compared with oleic acid as the capping ligand, *n*-butylamine, with its shorter chain length, provided stronger evidence for hole transfer from the CdSe nanocrystals to MDMO-PPV.[53] A polyfluorene copolymer, poly[2,7-(9,9-dioctyl-fluorene)-*alt*-5,5-(4′,7′-di-2-thienyl-2′,1′,3′-benzothiadiazole)] (APFO-3),[54] was developed by tuning the chemical structures in the conjugated backbones to harvest more photons over the entire solar spectrum. A strongly electron-withdrawing moiety, 2,1,3-benzothiadiazole, was copolymerized with an electron-donating unit to form poly[2,6-(4,4-bis-(2-ethylhexyl)-4*H*-cyclopenta[2,1-*b*;3,4-*b*′]dithiophene)-*alt*-4,7-(2,1,3-benzothiadiazole)] (PCPDTBT). When 10 wt% PCPDTBT was incorporated into the active layer, the CdSe nanocrystals and the PCPDTBT polymer components absorbed strongly in the ranges 350–450 and 630–720 nm, respectively. The resulting device exhibited a maximum EQE of 55% and a certified PCE of 3.1%,[55] with elimination of unwanted holes leakage into the cathode when a ZnO buffer layer was present.[56] Using time-resolved spectroscopic techniques, it was found that the carrier recombination dynamics depended strongly on the charge density and not on the electric field, a phenomenon that was related to the capping agents or the defects at the surface between the semiconductor nanocrystals and the polymer.[57] Another electron-withdrawing moiety, the thieno[3,4-*c*]pyrrole-4,6-dione (TPD) unit, having a symmetrical, rigidly fused, and coplanar structure, is also beneficial for solar cells when it is incorporated in conjugated polymers.[58] The conjugated polymer PDTTTPD, comprising 2,5-di(thiophen-2-yl)thieno[3,2-*b*]thiophene and TPD moieties, has been incorporated into CdSe tetrapods to investigate the effects of thermal annealing on morphology and device performance.[59]

2.3. Lead-Based Nanocrystals

PbS nanocrystal QDs exhibit tunable broad band absorption, equal confinement of electrons and holes, and long-lived excited states. A device prepared with MEH-PPV/PbS as a nanocomposite material demonstrated the harvesting of infrared-photogenerated carriers, a photovoltaic effect across the spectral region from 800 to 2000 nm,[60] and a PCE of 0.7% at an incident light power of 5 mW cm^{-2}.[61] **Table 2** lists all the device characterization data reported for nanocomposite solar cells incorporating polymer/Pb–based QD blends. Low band gap polymers containing *N*-alkyldithienopyrrole moieties, such as poly(2,3-didecyl-quinoxaline-5,8-diyl-*alt*-*N*-octyldithieno[3,2-*b*:2',3'-*d*]pyrrole) (PDTPQx)[62] and poly[2,6-(*N*-(1-octylnonyl)dithieno[3,2-*b*:2',3'-*d*]pyrrole)-*alt*-4,7-(2,1,3-benzothiadiazole)] (PDTPBT),[63] have been blended with PbS QDs and incorporated with a TiO_2 buffer layer to improving the maximum PCE up to 3.8%. Photoinduced absorption spectroscopy provided evidence for long-lived, microseconds to milliseconds, positive polarons on the conjugated polymer, PDTPQx-HD, following selective photoexcitation of the PbS QDs.[64,65] A novel process has been reported for a PDPPTPT/PbS nanocomposite solar cell device fabricated without using poly(3,4-ethylenedioxythiophene):polystyrenesulfonate (PEDOT:PSS) as the hole transporting layer. Rather than employing a traditional long reaction time for ligand exchange, the active layer (PDPPTPT/PbS) was soaked several times in an acetonitrile solution of 1,4-benzenedithiol to replace the oleic acid ligands.[66]

Schottky junction solar cells incorporating ternary PbS_xSe_{1-x} QDs have displayed a relatively high V_{oc} of 0.4V from their PbS QDs (x = 1) and high J_{sc} of 21 mA cm^{-2}[67] from their PbSe QDs (x = 0), achieving PCEs of up to 3.3%.[68] The BHJ device can be further improved by using a mixture nanostructures of QDs and nanorods with PbS_xSe_{1-x}[69] or PbS QDs blended with PSBTBT.[70] A low band gap (E_g = 1.7eV) polymer, PTB1, introduced into the PbS QDs phase exhibited the highest PCE of 2.8% when the PbS QDs were reduced to a size having a corresponding band gap energy of 1.32 eV.[71] A series of alternative planar bilayer structure of poly(3-octylthiophene)/PbS solar cells has been developed since 2005,[72] achieving a PCE of 4.2% after controlling the thickness of the polymer and QDs to 15 and 90 nm, respectively.[73]

When the S atoms are substituted by Se atoms, charge carrier kinetics probed with femtosecond transient absorption demonstrates that PbSe QDs has potential to exceed the

theoretical maximum thermodynamic conversion efficiency.[5,74] PbSe QDs has also been blended with the polymers P3HT and MEH-PPV for use as the active layer for the nanocomposite solar cells.[75,76] These polymer/PbSe devices exhibited lower PCEs because of the absent of photoinduced CT in devices based on MDMO-PPV/PbSe and P3HT/PbSe.[77] Therefore, most PbSe QDs have been based on Schottky junction structures, which rely on the built-in field driving extraction of electrons between the indium tin oxide and the back contact (Mg or Al).[78–83] Recently, depleted-heterojunction–type PbSe QDs solar cells incorporating transparent TiO_2 contacts have led to significantly breakthroughs in PCEs (>7%).[84–87]

3. Photocatalysis Applications

In the past decade, several kinds of conducting polymers, including polyaniline (PANI),[88–107] P3HT,[108–115] polypyrrole (PPy),[116–128] PEDOT,[129–133] and others,[134–147] have been used in the preparation of photocatalysts based on polymer/semiconductor nanocrystal nanocomposites. With suitable energy levels, conducting polymers can sensitize semiconductor nanocrystals to improve the light harvesting efficiency as well as promote effective charge separation to increase the carrier utilization efficiency. Both of these two merits are beneficial for photocatalytic applications. Semiconductor photocatalysts are usually in the form of powder, which possess large surface areas when dispersed in the reaction solution. There remain, however, several drawbacks affecting the practical use of powdery semiconductor photocatalysts: (i) time-consuming procedures for retracting photocatalysts from the reaction solution, and the inevitable loss of photocatalysts;[148] (ii) the dust of powdery photocatalyst is a risk factor to human health; [149] (iii) photocatalyst aggregation decreases the total surface area during the photocatalytic reaction, and decreases the photocatalytic activity.[150] An effective strategy to solve these problems is to immobilize the photocatalysts on a polymeric support. The ideal polymeric support should satisfy several features: good adhesion with the photocatalyst; [151] a large specific surface area; high adsorption capability toward the reaction species; high chemical inertness; and good mechanical stability. Several methods have been developed to immobilize photocatalysts on polymeric supports, including electrospinning,[152–155] sol–gel methods,[156–163] atomic layer deposition,[164–166] solvent-casting process,[167,168] hydrothermal methods,[169–172] solvothermal methods,[173] solution polymerization,[174–176] ion exchange,[150,177–181] and impregnation.[149,182,183] Most of these methods can be performed at relatively low temperature to avoid damage to the polymeric supports.

3.1. Polymer-Sensitized TiO2-Based Composite Photocatalysts

TiO_2 is the most widely studied photocatalyst because of its chemical stability, nontoxicity, and relatively low cost. Nevertheless, the large bandgap of TiO_2 limits its light absorption to only 5% of the solar spectrum. Coupling with a conducting polymer having a narrow band gap is an effective means of extending the light absorption spectrum of TiO_2 and, thereby, improving the photocatalytic activity. Luo et al.[140] modified TiO_2 nanoparticles with conjugated derivatives of polyisoprene (CDPIP) using a delicate bromine addition/dehydrobromination approach. The as-prepared TiO_2/CDPIP composite photocatalyst exhibited notable photocatalytic performance under illumination with visible light; **Figure 7**a

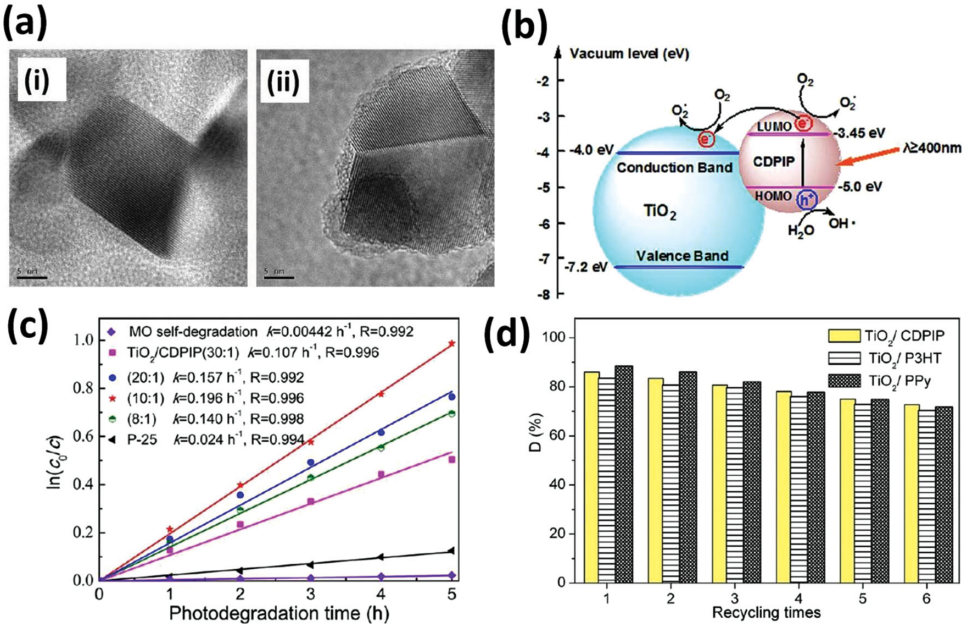

Figure 7. a) HRTEM images of i) TiO_2 and ii) TiO_2/CDPIP. b) Relative band structures of TiO_2/CDPIP and the proposed CT processes for MO degradation. c) Photocatalytic degradation of MO in the presence of P-25 TiO_2 and TiO_2/CDPIP at various TiO_2/CDPIP ratios. d) Recycling tests on TiO_2/CDPIP for MO degradation. Reproduced with permission.[140] Copyright 2012, American Chemical Society.

NANO MICRO small

displays the high resolution TEM (HRTEM) of i) TiO_2 and ii) TiO_2/CDPIP. Figure 7b presents the possible photocatalytic mechanism for the enhanced visible light photocatalytic activity of TiO_2/CDPIP nanocomposites. CDPIP readily absorbs visible light to induce a π–π^* transition and produce electron/hole pairs. Because of the band offset, the excited state electrons in the LUMO of CDPIP (–3.45 eV) readily transferred to the conduction band of TiO_2 (–4.0 eV) to achieve efficient charge separation. Figure 7c shows the photocatalytic experiments revealing that TiO_2/CDPIP nanocomposites exhibited significantly higher photocatalytic activities for the degradation of methyl orange (MO) than TiO_2 under irradiation with visible light. The rate constant of MO degradation was the highest (k = 0.196 h^{-1}) at the condition of TiO_2/CDPIP (10:1). A greater number of CDPIP molecules attached to the surfaces of the TiO_2 nanoparticles resulted in more visible light being absorbed to produce more electron/hole pairs. When the content of CDPIP on the TiO_2 surface exceeded a critical value, however, injection of electrons from the LUMO of CDPIP into the conduction band of TiO_2 became difficult because the electrons photogenerated at the outermost layer needed to travel a long distance to arrive at the TiO_2 surface. As a result, the photocatalytic activity of TiO_2/CDPIP first increased and then decreased upon increasing the content of CDPIP. Figure 7d shows the photocatalytic activity of TiO_2/CDPIP (10:1) composite maintained 80% for the first cycling run, indicating that the photocatalytic stability of the investigated nanocomposites is high and similar to those for TiO_2/PPy and TiO_2/P3HT nanocomposites.

Subsequently, a surfactant-directed in situ chemical polymerization method was used to synthesize PPy-decorated Ag-TiO_2 nanofibers (PPy-Ag-TiO_2).[125] **Figure 8**a shows the as-synthesized PPy-Ag-TiO_2 nanofibers exhibited remarkable photocatalytic performance for the decomposition of gaseous acetone under illumination with visible light. Figure 8b shows the relatively low PL intensity of PPy-Ag-TiO_2, indicating substantially low rate of recombination of the charge carriers. Figure 8c presents the photocurrents with an order of PPy-Ag-TiO_2 > PPy-TiO_2 > Ag-TiO_2 > pure TiO_2. PL spectra and photocurrent measurement both suggested the occurrence of more effective charge carrier separation for PPy-Ag-TiO_2. Figure 8d shows the PPy-Ag-TiO_2 nanofibers with significantly enhanced photocatalytic activity. Such enhancement was due to the improved visible light harvesting, rapid CT, and a low probability of electron/hole recombination, based on the synergistic effect of TiO_2, Ag, and PPy. When the PPy-Ag-TiO_2 nanofibers were illuminated under visible light, electrons were excited from the HOMO to the LUMO of PPy, leaving holes behind in the HOMO of PPy. The excited state electrons were readily injected into the conduction band of TiO_2 and further injected into the Fermi level of Ag. Figure 8e shows the recycling test of gaseous acetone degradation for PPy-Ag-TiO_2 nanofibers. The photocatalytic activity has no decreasing because of the large length-to-diameter ratios of the nanofiber structures.

3.2. Polymer-Sensitized ZnO-Based Composite Photocatalysts

Although TiO_2 is the most widely employed photocatalyst, ZnO appears to be a suitable alternative in some applications. Compared with TiO_2, ZnO can absorb a larger portion of the UV spectrum, and it exhibits superior photocatalytic properties.[184–186] Coupling ZnO with a narrow band gap conducting polymer is also an effective means of promoting charge carrier separation and improving the utilization of solar light. A facile chemisorption method together with a cold plasma treatment technique was applied to prepare the PANI-hybridized ZnO photocatalyst.[107] **Figure 9**a shows the PANI was uniformly coated on the ZnO surface with an intimate contact. Interestingly, the coated PANI acted cooperatively with deliberately introduced defects of ZnO (oxygen vacancy, V_o, and interstitial zinc, Zn_i) to enhance the resulting photocatalytic efficiency. Figure 9b shows the degradation of MO photocatalyzed by pure ZnO (Z), defective ZnO (Z-D),

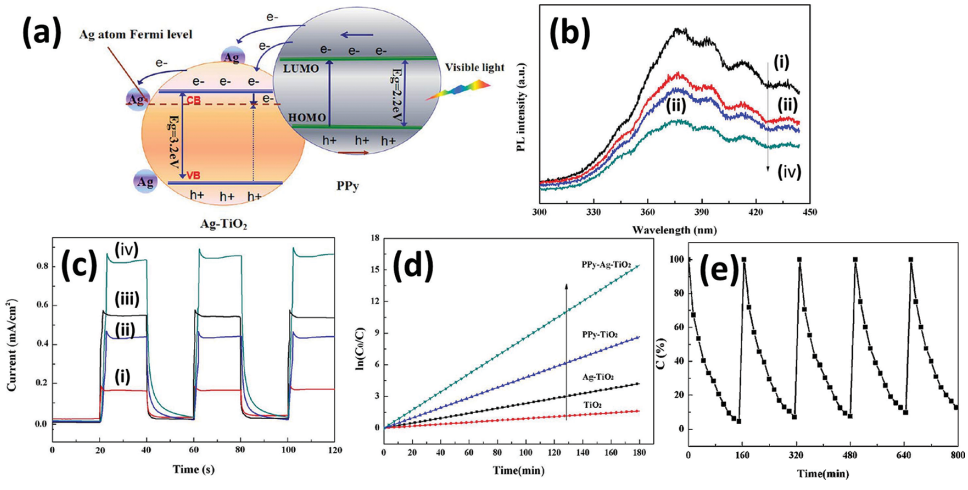

Figure 8. a) Relative band structures of PPy-Ag-TiO_2 and the proposed CT processes. b) PL emission spectra and c) photocurrent transient responses for i) TiO_2, ii) Ag-TiO_2, iii) PPy-TiO_2, and iv) PPy-Ag-TiO_2. d) Photocatalytic activities of various samples toward gaseous acetone degradation under visible irradiation. e) Recycling tests for PPy-Ag-TiO_2 in acetone degradation. Reproduced with permission.[125] Copyright 2013, American Chemical Society.

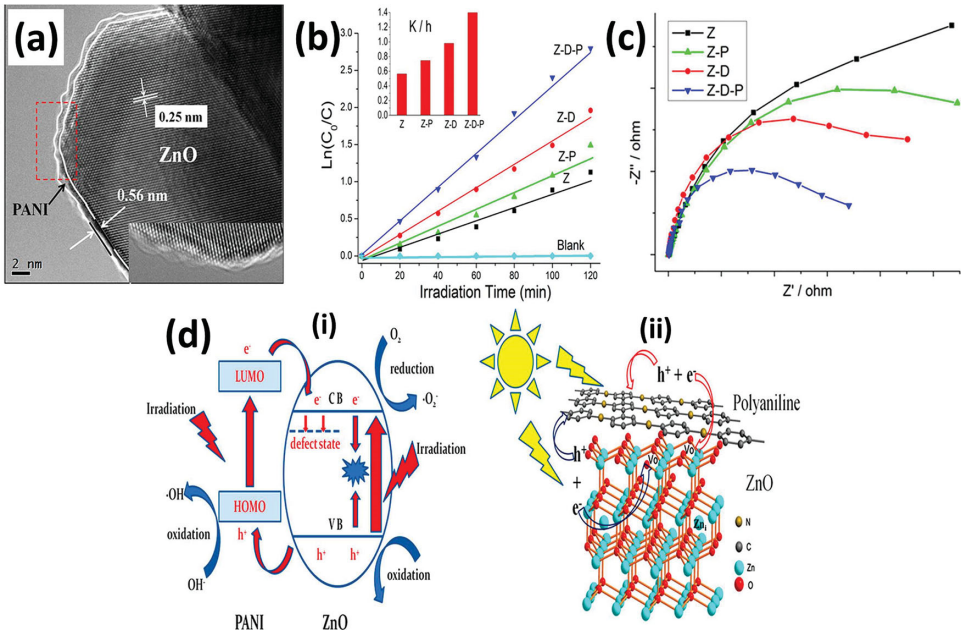

Figure 9. a) HRTEM image of Z-D-P; inset: amorphous edge of the coated PANI. b) Photocatalytic degradation of MO over various samples under UV irradiation; inset: corresponding rate constants of MO degradation. c) EIS Nyquist plots for various samples under irradiation with UV light. d-i) Relative band structures of PANI/ZnO and the proposed CT processes for MO degradation. ii) Schematic diagram illustrating the synergistic effect between defects and PANI. Reproduced with permission.[107] Copyright 2014, American Chemical Society.

PANI-hybridized ZnO (Z-P), and PANI-hybridized defective ZnO (Z-D-P). The Z-D-P composite photocatalyst exhibited significantly enhanced photocatalytic activity, with a rate constant for MO degradation 2.5 times higher than that of pure ZnO. Figure 9c shows that the electrochemical impedance spectroscopy (EIS) study revealed that both defects and PANI led to more efficient charge separation and faster interfacial CT. A synergistic effect between PANI and defects was proposed as a probable mechanism to account for the enhanced photocatalytic activity. Figure 9d-i displays a schematic diagram describing the well match energy band of PANI and ZnO. Under illumination with light, the photogenerated holes transferred from ZnO toward the PANI monolayer, while the photoexcited electrons from both ZnO and PANI could be trapped by V_o at the surface (Figure 9d-ii). The surficial V_o acted as trapping sites for photoexcited electron and also as active sites for reaction species, both of which are beneficial for photocatalytic reactions. Consequently, significantly enhanced photocatalytic performance was achieved by the Z-D-P nanocomposite photocatalyst.

3.3. Other Types of Polymer-Sensitized Composite Photocatalysts

In addition to TiO_2 and ZnO, many other semiconductors with notable photocatalytic properties have been studied intensively, including CdS, Si, and C_3N_4. CdS is one of the most popular visible-light-driven photocatalysts because it has band gap energy of 2.5 eV. Furthermore, its conduction band at relatively negative potential (–1.0 versus NHE) offers CdS good photocatalytic activities. The significantly enhanced photocatalytic activity of PANI-CdS composite photocatalysts for the evolution of hydrogen was demonstrated.[102] A series of nanocomposite catalysts, denoted as PANI-CdS-1, PANI-CdS-2, PANI-CdS-3, PANI-CdS-4 and PANI-CdS-5, represent the molar ratio of PANI and CdS fixing at 0.5, 0.7, 1, 1.5, and 2. **Figure 10**a shows PANI-CdS-1 with a much higher rate of hydrogen production than pure CdS and other various photocatalysts. Figure 10b exhibits the PANI-CdS-1 was considerably stable during the photocatalytic process; no appreciable decay in the rate of hydrogen evolution could be observed after 20 h of light irradiation. Two reasons may be responsible for the remarkable photocatalytic properties

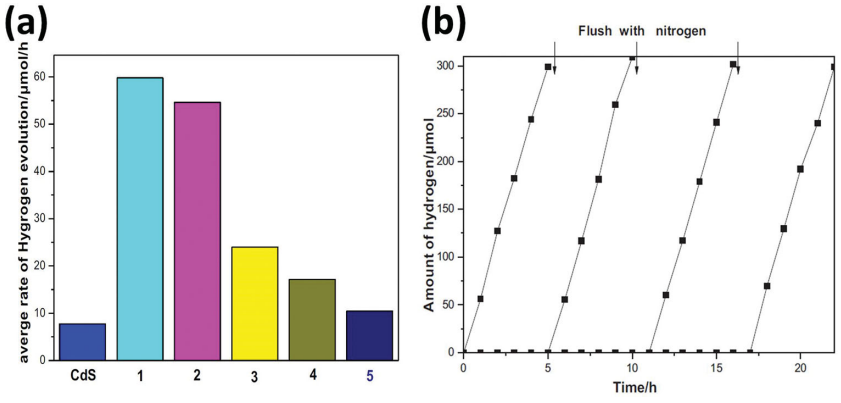

Figure 10. a) Rates of hydrogen evolution over CdS and PANI-CdS composite photocatalysts, with different PANI contents, under irradiation with visible light. b) Recycling tests for hydrogen evolution over PANI-CdS-1. Reproduced with permission.[102] Copyright 2012 International Association for Hydrogen Energy.

NANO MICRO small

of PANI-CdS: i) the photoexcited electrons transfer from PANI to CdS, giving rise to an increased amount of electrons available for hydrogen evolution; ii) PANI effectively prevents the agglomeration of CdS particles, which makes electron transfer from PANI to CdS become easy. However, the hydrogen evolution rate of PANI-CdS nanocomposite photocatalyst gradually decreased with the increasing PANI amount. The excess loading of PANI reduced the content of CdS and decreased photocatalytic activity.

Crystalline Si is very applicable for photoelectrochemical water splitting because its band gap (1.12 eV) is an ideal match for the solar spectrum.[132] Coating with a thin layer of conducting polymer has been proven to effectively stabilize Si-based photoelectrodes and prevent photocorrosion. **Figure 11**a shows i) the SEM image of Si/PEDOT core/shell nanowire arrays and ii) HRTEM image of the Si/PEDOT interface. Prior to PEDOT polymerization, the Si nanowires were modified with (3-aminopropyl)triethoxysilane (APS) to improve the PEDOT adhesion; an amorphous PEDOT shell formed on the crystalline Si nanowire core. The PEDOT layer performed three roles: as a multifunctional coating to prevent photocorrosion of the Si nanowires, to collect photogenerated holes, and to catalyze the water oxidation reaction. Figure 11b depicts the CT mechanism of a Si/PEDOT composite photoanode during photoelectrochemical water splitting. The incident light is absorbed mostly by the Si nanowires, due to the high transparency of PEDOT over the visible light range, to generate electron/hole pairs. The photogenerated electrons move along the Si nanowires to the Pt electrode via the external circuit to evolve hydrogen, while the photogenerated holes transfer to the PEDOT shell where they take part in the water oxidation reactions. Figure 11c-i shows the current density versus bias potential characteristics (*J–V* curves) for pure Si and Si/PEDOT electrodes recorded in 1 M KOH in the dark and under light illumination (AM 1.5G, 100 mW cm^{-2}). The *J–V* curve of pure Si showed a pronounced electrochemical oxidation of Si from –0.5 to 0.0 V (vs SCE). Both Si/PEDOT and Si-APS/PEDOT electrodes exhibited significant photoresponse, indicating that PEDOT layer effectively collected photogenerated holes to carry out the water oxidation reaction. Figure 11c-ii shows the photocurrent of pure Si nanowires decayed quickly because Si nanowires were completely corroded in few minutes. On the contrast, the photocurrent decay of Si/PEDOT and Si-APS/PEDOT composite electrodes was greatly deferred, indicating that the PEDOT layer protected the Si nanowires from photocorrosion.

3.4. Polymer-Immobilized TiO2-Based Composite Photocatalysts

Zeng et al.[158] prepared TiO_2/cellulose nanocomposite films using a sol–gel method through the hydrolysis of precursor TiO_2 sol solutions in regenerated cellulose (RC) films. **Figure 12**a shows the porous RC substrate providing cavities for the growth and immobilization of TiO_2 nanoparticles through electrostatic and hydrogen bonding interactions.

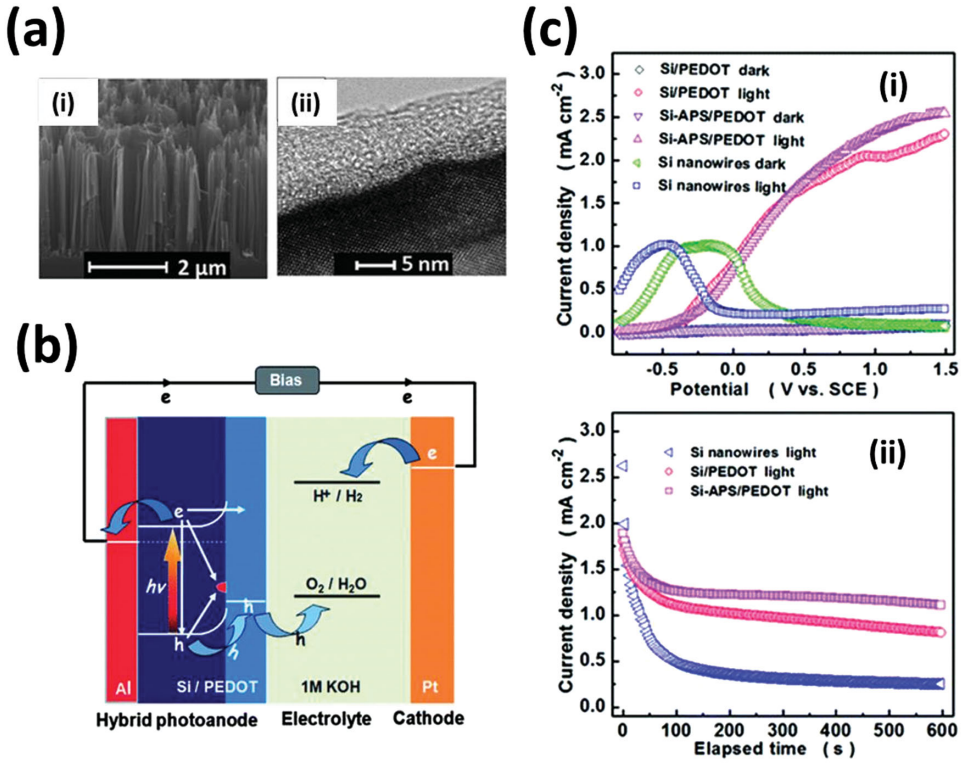

Figure 11. a-i) SEM and ii) HRTEM images of Si/PEDOT nanowires. b) Relative band structures of Si/PEDOT and the proposed CT processes for photoelectrochemical water splitting. c-i) *J–V* curves of various photoanodes recorded in 1 M KOH in the dark and under light illumination (AM 1.5 G, 100 mW cm^{-2}) and ii) *J–t* curves of different photoelectrodes recorded at a fixed potential of +0.5 V (vs SCE). Reproduced with permission.[132] Copyright 2013, Royal Chemical Society.

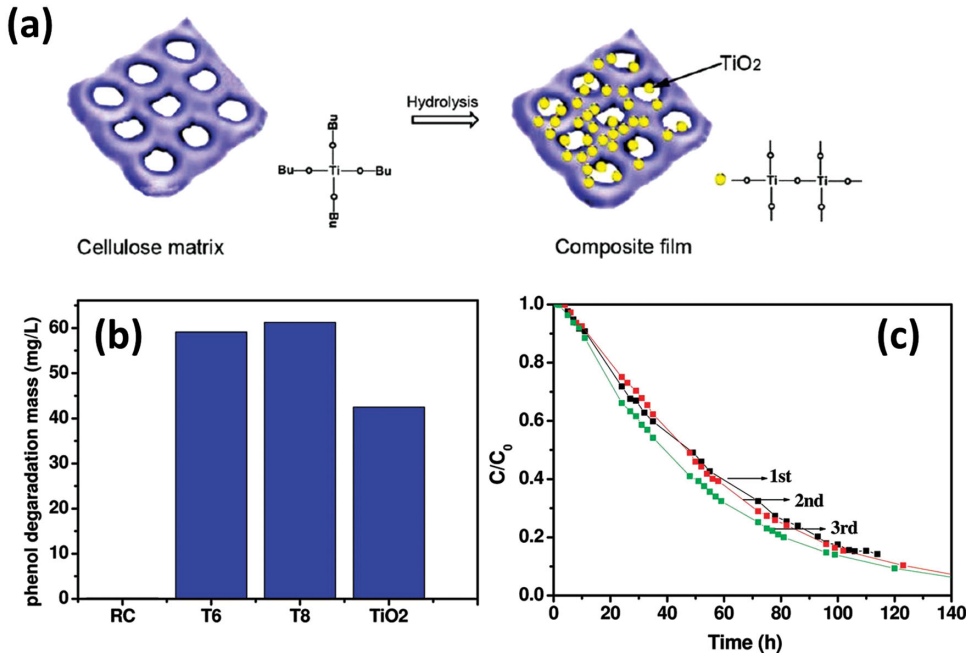

Figure 12. a) Schematic representation of the growth and immobilization of TiO_2 nanoparticles in an RC matrix. b) Phenol photodegradation behavior of various samples under UV irradiation for 120 h. T6 and T8 represent TiO_2/RC composite films prepared from different volumes of the sol solution. c) Recycling tests of TiO_2/RC films for phenol degradation. Reproduced with permission.[158] Copyright 2010, American Chemical Society.

Figure 12b shows these TiO_2/RC composite films exhibited notable photocatalytic performance for the degradation of phenol under irradiation with weak UV light; their photocatalytic activities were even comparable to that of anatase TiO_2 nanoparticles under the same experimental conditions, suggesting that the structure and properties of the TiO_2 nanoparticles were protected effectively. Moreover, Figure 12c shows the TiO_2/RC composite films had good mechanical properties, allowing them to be used as recyclable catalysts for the photodegradation of organic pollutants.

3.5. Polymer-Immobilized ZnO-Based Composite Photocatalysts

An atomic layer deposition (ALD) approach was used to either decorate nylon nanofibers with ZnO nanoparticles or to coat nylon nanofibers with a thin layer of ZnO, depending on the ALD parameters.[165] When highly dense ZnO nanoparticles were decorated upon the nylon nanofibers, they exhibited higher efficiency for the photocatalytic decomposition of Rhodamine B (RhB), due to their large surface area. In addition to the ALD approach, the hydrothermal method is another practical method for immobilizing ZnO on polymeric supports. A combination of electrospinning and hydrothermal methods was employed for the preparation of hierarchical composites featuring oriented ZnO nanowires grown around electrospun nanofibers.[171] The electrospun nanofibers were composed of cellulose acetate (CeAc), polyvinyl acetate (PVAc), and polyethylene glycol (PEG). These hierarchical composites were highly effective photocatalysts, as evidenced by the almost complete removal of the test pollutant, methylene blue, after 30 min of UV irradiation. Because the ZnO nanowires were grown on the CeAc/PVAc/PEG polymeric supports, the need for separation of the photocatalyst from the reaction solution was eliminated.

3.6. Other Types of Polymer-Immobilized Composite Photocatalysts

Figure 13a shows that D201, a macroporous resin of polystyrene-divinylbenzene matrix, was adopted as a support to fabricate D201-CdS composite photocatalysts using an ion exchange process.[179] Figure 13b displays the as-obtained D201-CdS beads were yellow, characteristic of the light absorption of CdS. Figure 13c exhibits the composite photocatalysts exhibited excellent photocatalytic activity for the degradation of RhB under irradiation with visible light. Furthermore, the photocorrosion of CdS was inhibited after immobilization within the D201 matrix. Figure 13d shows the D201-CdS composite photocatalysts employed for repeated use without noticeable loss in efficiency; in addition, they could be separated readily from the reaction solutions through simple filtration, suggesting their use as promising photocatalysts for practical applications in environmental remediation.

4. Conclusion

Conjugated polymer/nanocrystal QDs solar cells can exhibit PCEs of over 4% when using Cd- and Pb-based nanocrystals. Control over the polymer–nanocrystal QDs interface is a crucial factor affecting device performance. From a commercial point of view, postproduction treatment (ligand

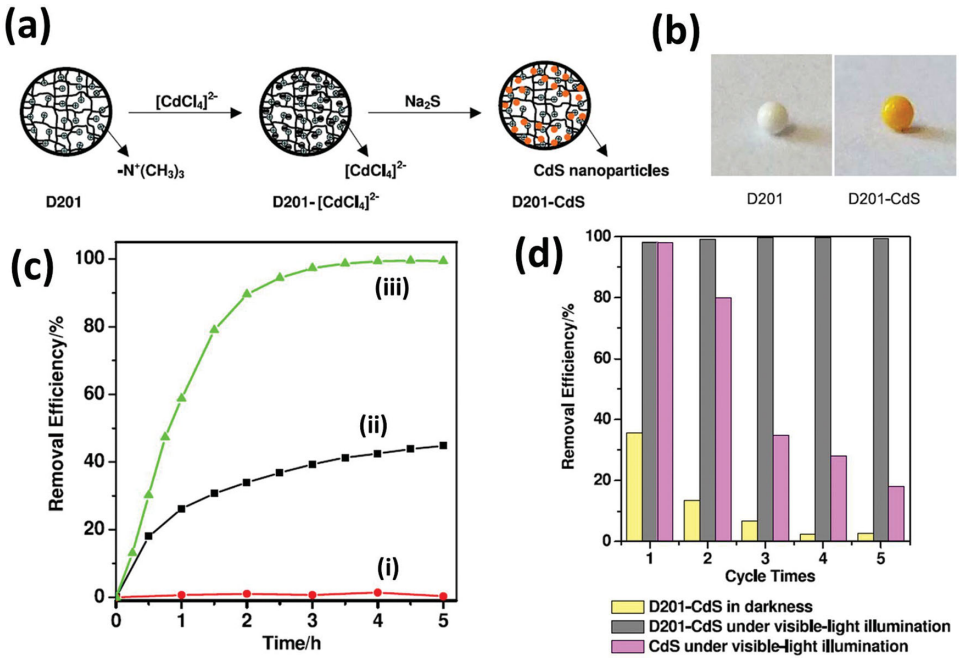

Figure 13. a) Schematic representation of the preparation of a D201-CdS composite photocatalyst. b) Photographs of pure D201 and D201-CdS. c) RhB degradation under various conditions: i) in the absence of D201-CdS, ii) in the presence of D201-CdS in the dark, and iii) in the presence of D201-CdS under irradiation with visible light. d) Recycling tests of CdS and D201-CdS for the degradation of RhB. Reproduced with permission.[179] Copyright 2011, IOP Publishing.

exchange; washing with acids) and methods for film formation (solvents choice) are considered more straightforward and tunable fabrication processes for improving efficiency. It is also important to completely remove the capping ligands from the surfaces of the nanocrystal QDs to ensure more-intimate contact with the conjugated polymer. Such novel approaches include polymer grafting and the in situ synthesis of nanocrystal QDs in polymer solutions or polymer films. These methods can provide important information regarding charge generation and recombination in highly efficient next-generation devices. After optimization of device efficiency, long-term stability is an issue that must be considered to minimize oxidation on the nanocrystals' surfaces. For photocatalysis using nanocrystal composites, structural and band gap engineering are both necessary to further improve light absorption from the solar spectrum. A fundamental understanding of the CT processes occurring in composite photocatalysts will be critical for maximizing the carrier utilization efficiency in photocatalytic systems. Furthermore, developing generalized synthetic processes for solar fuel production in industrial settings will be the most important challenge for the practical applicability of reliable polymer/semiconductor nanocrystal composites.

[1] M. Helgesen, R. Sondergaard, F. C. Krebs, *J. Mater. Chem.* **2010**, *20*, 36.
[2] J. Boucle, P. Ravirajan, J. Nelson, *J. Mater. Chem.* **2007**, *17*, 3141.
[3] O. E. Semonin, J. M. Luther, M. C. Beard, *Mater. Today* **2012**, *15*, 508.
[4] M. A. Green, *Third Generation Photovoltaics*, Springer, Berlin-Heidelberg **2003**.
[5] R. D. Schaller, M. A. Petruska, V. I. Klimov, *Appl. Phys. Lett.* **2005**, *87*, 253102.
[6] R. J. Ellingson, M. C. Beard, J. C. Johnson, P. Yu, O. I Micic, A. J. Nozik, A. Shabaev, A. L. Efros, *Nano Lett.* **2005**, *5*, 865.
[7] J. J. H. Pijpers, R. Ulbricht, K. J. Tielrooij, A. Osherov, Y. Golan, C. Delerue, G. Allan, M. Bonn, *Nat. Phys.* **2009**, *5*, 811.
[8] D. Qi, M. Fischbein, M. Drndi , S. Šelmi , *Appl. Phys. Lett.* **2005**, *86*, 093103.
[9] A. J. Moule, L. Chang, C. Thambidurai, R. Vidu, P. Stroeve, *J. Mater. Chem.* **2012**, *22*, 2351.
[10] T. Xu, Q. Qiao, *Energy Environ. Sci.* **2011**, *4*, 2700.
[11] F. Gao, S. Ren, J. Wang, *Energy Environ. Sci.* **2013**, *6*, 2020.
[12] J. Patel, F. Mighri, A. Ajji, T. K. Chaudhuri, *Nano Energy* **2014**, *5*, 36.
[13] J. Albero, J. N. Clifford, E. Palomares, *Coord. Chem. Rev.* **2014**, *263–264*, 53.
[14] J. N. Freitas, A. S. Goncalves, A. F. Nogueira, *Nanoscale* **2014**, *6*, 6371 .
[15] Y. Park, R. C. Advincula, *Chem. Mater.* **2011**, *23*, 4273.
[16] X. Chen, S. Shen, L. Guo, S. S. Mao, *Chem. Rev.* **2010**, *110*, 6503.
[17] A. Furube, L. Du, K. Hara, R. Katoh, M. Tachiya, *J. Am. Chem. Soc.* **2007**, *129*, 14852
[18] S. K. Cushing, J. Li, F. Meng, T. R. Senty, S. Suri, M. Zhi, M. Li, A. D. Bristow, N. Wu, *J. Am. Chem. Soc.* **2012**, *134*, 15033.
[19] P. A. DeSario, J. J. Pietron, D. E. DeVantier, T. H. Brintlinger, R. M. Stroud, D. R. Rolison, *Nanoscale* **2013**, *5*, 8073.
[20] N. Zhang, S. Liu, Y.-J. Xu, *Nanoscale* **2012**, *4*, 2227.
[21] Y. Qu, X. Duan, *Chem. Soc. Rev.* **2013**, *42*, 2568.
[22] Y. Wang, Q. Wang, X. Zhan, F. Wang, M. Safdar, J. He, *Nanoscale* **2013**, *5*, 8326.
[23] S. R. Forrest, *Nature* **2004**, *428*, 911.
[24] Y.-W. Su, S.-C. Lan, K.-H Wei, *Mater. Today* **2012**, *15*, 554.
[25] J.-M. Jiang, M.-C. Yuan, K. Dinakaran, A. Hariharan, K.-H. Wei, *J. Mater. Chem. A* **2013**, *1*, 4415.
[26] L. Manna, E. C. Scher, A. P. Alivisatos, *J. Am. Chem. Soc.* **2000**, *122*, 12700.

[27] X. Peng, L. Manna, W. Yang, J. Wickham, E. Scher, A. Kadavanich, A. P. Alivisatos, *Nature* **2000**, *404*, 59.
[28] P. Reiss, J. Bleuse, A. Pron, *Nano Lett.* **2002**, *2*, 781.
[29] E. Zillner, S. Fengler, P. Niyamakom, F. Rauscher, K. Köhler, T. Dittrich, *J. Phys. Chem. C* **2012**, *116*, 16747.
[30] N. C. Greenham, X. Peng, A. P. Alivisatos, *Phys. Rev. B* **1996**, *54*, 17628.
[31] Y. Wang, *Nature* **1992**, *356*, 585.
[32] A. Biebersdorf, R. Dietmüller, A. S. Susha, A. L. Rogach, S. K. Poznyak, D. V. Talapin, H. Weller, T. A. Klar, J. Feldmann, *Nano Lett.* **2006**, *6*, 1559.
[33] P. Brown, P. V. Kamat, *J. Am. Chem. Soc.* **2008**, *130*, 8890.
[34] J. H. Bang, P. V. Kamat, *ACS Nano* **2011**, *5*, 9421.
[35] A. K. Bansal, F. Antolini, M. T. Sajjad, L. Stroea, R. Mazzaro, S. G. Ramkumar, K. J. Kass, S. Allard, U. Scherf, I. D. W. Samuel, *Phys. Chem. Chem. Phys.* **2014**, *16*, 9556.
[36] W. U. Huynh, X. Peng, A. P. Alivisatos, *Adv. Mater.* **1999**, *11*, 923.
[37] W. U. Huynh, J. J. Dittmer, A. P. Alivisatos, *Science* **2002**, *295*, 2425.
[38] I. Gur, N. A. Fromer, C.-P. Chen, A. G. Kanaras, A. P. Alivisatos, *Nano Lett.* **2006**, *7*, 409.
[39] B. Sun, N. C. Greenham, *Phys. Chem. Chem. Phys.* **2006**, *8*, 3557.
[40] J. D. Olson, G. P. Gray, S. A. Carter, *Sol. Energy Mater. Sol. Cells* **2009**, *93*, 519.
[41] J. Yang, A. Tang, R. Zhou, J. Xue, *Sol. Energy Mater. Sol. Cells* **2011**, *95*, 476.
[42] Y. Zhou, F. S. Riehle, Y. Yuan, H. F. Schleiermacher, M. Niggemann, G. A. Urban, M. Krüger, *Appl. Phys. Lett.* **2010**, *96*, 013304.
[43] J. Albero, P. Riente, J. N. Clifford, M. A. Pericàs, E. Palomares, *J. Phys. Chem. C* **2013**, *117*, 13374.
[44] L. Qian, J. Yang, R. Zhou, A. Tang, Y. Zheng, Tseng, T.-K. D. Bera, J. Xue, P. H. Holloway, *J Mater Chem* **2011**, *21*, 3814.
[45] S. Ren, L.-Y. Chang, S.-K. Lim, J. Zhao, M. Smith, N. Zhao, V. Bulović, M. Bawendi, S. Gradečak, *Nano Lett.* **2011**, *11*, 3998.
[46] R. Zhou, R. Stalder, D. Xie, W. Cao, Y. Zheng, Y. Yang, M. Plaisant, P. H. Holloway, K. S. Schanze, J. R. Reynolds, J. Xue, *ACS Nano* **2013**, *7*, 4846.
[47] M. D. Heinemann, K. Von Maydell, F. Zutz, J. Kolny-Olesiak, H. Borchert, I. Riedel, J. Parisi, *Adv. Funct. Mater.* **2009**, *19*, 3788.
[48] D. S. Ginger, N. C. Greenham, *Phys. Rev. B* **1999**, *59*, 10622.
[49] B. Sun, E. Marx, N. C. Greenham, *Nano Lett.* **2003**, *3*, 961.
[50] B. Sun, H. J. Snaith, A. S. Dhoot, S. Westenhoff, N. C. Greenham, *J. Appl. Phys.* **2005**, *97*, 014914.
[51] H. J. Snaith, G. L. Whiting, B. Sun, N. C. Greenham, W. T. S. Huck, R. H. Friend, *Nano Lett.* **2005**, *5*, 1653.
[52] M. L. Böhm, R. J. P. Kist, F. S. F. Morgenstern, B. Ehrler, S. Zarra, A. Kumar, Y. Vaynzof, N. C. Greenham, *Adv. Energy Mater.* **2014**, DOI 10.1002/aenm.201400139.
[53] F. S. F. Morgenstern, A. Rao, M. L. Böhm, R. J. P. Kist, Y. Vaynzof, N. C. Greenham, *ACS Nano* **2014**, *8*, 1647.
[54] P. Wang, A. Abrusci, H. M. P. Wong, M. Svensson, M. R. Andersson, N. C. Greenham, *Nano Lett.* **2006**, *6*, 1789.
[55] S. Dayal, N. Kopidakis, D. C. Olson, D. S. Ginley, G. Rumbles, *Nano Lett.* **2009**, *10*, 239–242.
[56] R. Zhou, Y. Zheng, L. Qian, Y. Yang, P. H. Holloway, J. Xue, *Nanoscale* **2012**, *4*, 3507.
[57] J. Albero, Y. Zhou, M. Eck, F. Rauscher, P. Niyamakom, I. Dumsch, S. Allard, U. Scherf, M. Kruger, E. Palomares, *Chem. Sci.* **2011**, *2*, 2396.
[58] Y. Zou, A. Najari, P. Berrouard, S. Beaupré, B. Réda Aïch, Y. Tao, M. Leclerc, *J. Am. Chem. Soc.* **2010**, *132*, 5330.
[59] C.-Y. Kuo, M.-S. Su, G.-Y. Chen, C.-S. Ku, H.-Y. Lee, K.-H. Wei, *Energy Environ. Sci.* **2011**, *4*, 2316.
[60] S. A. McDonald, G. Konstantatos, S. Zhang, P. W. Cyr, E. J. D. Klem, L. Levina, E. H. Sargent, *Nat. Mater.* **2005**, *4*, 138.
[61] A. A. R. Watt, D. Blake, J. H. Warner, E. A. Thomsen, E. L. Tavenner, H. Rubinsztein-Dunlop, P. Meredith,. *J. Phys. D: Appl. Phys.* **2005**, *38*, 2006.
[62] K. M. Noone, E. Strein, N. C. Anderson, P.-T. Wu, S. A. Jenekhe, D. S. Ginger, *Nano Lett.* **2010**, *10*, 2635.
[63] J. Seo, M. J. Cho, D. Lee, A. N. Cartwright, P. N. Prasad, *Adv. Mater.* **2011**, *23*, 3984.
[64] A. E. Colbert, E. M. Janke, S. T. Hsieh, S. Subramaniyan, C. W. Schlenker, S. A. Jenekhe, D. S. Ginger, *J. Phys. Chem. Lett.* **2012**, *4*, 280.
[65] E. Strein, A. Colbert, S. Subramaniyan, H. Nagaoka, C. W. Schlenker, E. Janke, S. A. Jenekhe, D. S. Ginger, *Energy Environ, Sci* **2013**, *6*, 769.
[66] C. Piliego, M. Manca, R. Kroon, M. Yarema, K. Szendrei, M. R. Andersson, W. Heiss, M. A. Loi, *J. Mater. Chem.* **2012**, *22*, 24411.
[67] J. M. Luther, M. Law, M. C. Beard, Q. Song, M. O. Reese, R. J. Ellingson, A. J. Nozik, *Nano Lett.* **2008**, *8*, 3488.
[68] W. Ma, J. M. Luther, H. Zheng, Y. Wu, A. P. Alivisatos, *Nano Lett.* **2009**, *9*, 1699.
[69] M. Nam, S. Kim, S. Kim, S.-W. Kim, K. Lee, *Nanoscale* **2013**, *5*, 8202.
[70] M. Nam, J. Park, S.-W. Kim, K. Lee, *J. Mater. Chem. A* **2014**, *2*, 3978.
[71] H. Nagaoka, A. E. Colbert, E. Strein, E. M. Janke, M. Salvador, C. W. Schlenker, D. S. Ginger, *J. Phys. Chem. C* **2014**, *118*, 5710.
[72] A. Maria, P. W. Cyr, E. J. D. Klem, L. Levina, E. H. Sargent, *Appl. Phys. Lett.* **2005**, *87*, 213112.
[73] Y. Zhang, Z. Li, J. Ouyang, S.-W. Tsang, J. Lu, K. Yu, J. Ding, Y. Tao, *Org. Electron.* **2012**, *13*, 2773–2780.
[74] R. D. Schaller, V. I. Klimov, *Phys. Rev. Lett.* **2004**, *92*, 186601.
[75] D. Cui, J. Xu, T. Zhu, G. Paradee, S. Ashok, M. Gerhold, *Appl. Phys. Lett.* **2006**, *88*, 183111.
[76] X. Jiang, R. D. Schaller, S. B. Lee, J. M. Pietryga, V. I. Klimov, A. A. Zakhidov, *J. Mater. Res.* **2007**, *22*, 2204.
[77] K. M. Noone, N. C. Anderson, N. E. Horwitz, A. M. Munro, A. P. Kulkarni, D. S. Ginger, *ACS Nano* **2009**, *3*, 1345.
[78] G. I. Koleilat, L. Levina, H. Shukla, S. H. Myrskog, S. Hinds, A. G. Pattantyus-Abraham, E. H. Sargent, *ACS Nano* **2008**, *2*, 833.
[79] C.-Y. Kuo, M.-S. Su, Y.-C. Hsu, H.-N. Lin, K.-H. Wei, *Adv. Funct. Mater.* **2010**, *20*, 3555.
[80] C.-Y. Kuo, M.-S. Su, C.-S. Ku, S.-M. Wang, H.-Y. Lee, K.-H. Wei, *J. Mater. Chem.* **2011**, *21*, 11605.
[81] N. Zhao, T. P. Osedach, L.-Y. Chang, S. M. Geyer, D. Wanger, M. T. Binda, A. C. Arango, M. G. Bawendi, V. Bulovic, *ACS Nano* **2010**, *4*, 3743.
[82] R. Debnath, J. Tang, D. A. Barkhouse, X. Wang, A. G. Pattantyus-Abraham, L. Brzozowski, L. Levina, E. H. Sargent, *J Am. Chem. Soc.* **2010**, *132*, 5952.
[83] W. Yoon, J. E. Boercker, M. P. Lumb, D. Placencia, E. E. Foos, J. G. Tischler, *Sci. Rep.* **2013**, *3*, 2225.
[84] A. G. Pattantyus-Abraham, I. J. Kramer, A. R. Barkhouse, X. Wang, G. Konstantatos, R. Debnath, L. Levina, I. Raabe, M. K. Nazeeruddin, M. Grätzel, E. H. Sargent, *ACS Nano* **2010**, *4*, 3374.
[85] J. Tang, K. W. Kemp, S. Hoogland, K. S. Jeong, H. Liu, L. Levina, M. Furukawa, X. Wang, R. Debnath, D. Cha, K. W. Chou, A. Fischer, A. Amassian, J. B. Asbury, E. H. Sargent, *Nat. Mater.* **2011**, *10*, 765.
[86] A. H. Ip, S. M. Thon, S. Hoogland, O. Voznyy, D. Zhitomirsky, R. Debnath, L. Levina, L. R. Rollny, G. H. Carey, A. Fischer, K. W. Kemp, I. J. Kramer, Z. Ning, A. J. Labelle, K. W. Chou, A. Amassian, E. H. Sargent, *Nat. Nanotechnol.* **2012**, *7*, 577.
[87] G.-H. Kim, B. Walker, H.-B. Kim, J. Y. Kim, E. H. Sargent, J. Park, J. Y. Kim, *Adv. Mater.* **2014**, *26*, 3321.

[88] X. Li, D. Wang, G. Cheng, Q. Luo, J. An, Y. Wang, *Appl. Catal. B: Environ.* **2008**, *81*, 267.
[89] H. Zhang, R. Zong, J. Zhao, Y. Zhu, *Environ. Sci. Technol.* **2008**, *42*, 3803.
[90] H. Zhang, Y. Zhu, *J. Phys. Chem. C* **2010**, *114*, 5822.
[91] M. A. Salem, A. F. Al-Ghonemiy, A. B. Zaki, *Appl. Catal. B: Environ.* **2009**, *91*, 59.
[92] M. Shang, W. Wang, S. Sun, J. Ren, L. Zhou, L. Zhang, *J. Phys. Chem. C* **2009**, *113*, 20228.
[93] D. Mahanta, U. Manna, G. Madras, S. Patil, *ACS Appl. Mater. Interfaces* **2011**, *3*, 84.
[94] T. Guo, L. Wang, D. G. Evans, W. Yang, *J. Phys. Chem. C* **2010**, *114*, 4765.
[95] G. Liao, S. Chen, X. Quan, Y. Zhang, H. Zhao, *Appl. Catal. B: Environ.* **2011**, *102*, 126.
[96] S. Ameen, M. S. Akhtar, Y. S. Kim, O-B. Yang, H.-S. Shin, *Colloid Polym. Sci.* **2011**, *289*, 415.
[97] S. Ameen, M. S. Akhtar, Y. S. Kim, H. S. Shin, *Chem. Eng. J.* **2012**, *181–182*, 806.
[98] Y. Wang, J. Xu, W. Zong, Y. Zhu, *J. Solid State Chem.* **2011**, *184*, 1433.
[99] V. Eskizeybek, F. Sarı, H. Gulce, A. Gulce, A. Avcı, *Appl. Catal. B: Environ.* **2012**, *119–120*, 197.
[100] A. Olad, S. Behboudi, A. A. Entezami, *Bull. Mater. Sci.* **2012**, *35*, 801.
[101] R. Nosrati, A. Olad, R. Maramifar, *Environ. Sci. Pollut. Res.* **2012**, *19*, 2291.
[102] K. He, M. Li, L. Guo, *Int. J. Hydrogen Energy* **2012**, *37*, 755.
[103] P. Xiong, Q. Chen, M. He, X. Sun, X. Wang, *J. Mater. Chem.* **2012**, *22*, 17485.
[104] P. Xiong, L. Wang, X. Sun, B. , Xu, X. Wang, *Ind. Eng. Chem. Res.* **2013**, *52*, 10105.
[105] Y. Lin, D. Li, J. Hu, G. Xiao, J. Wang, W. Li, X. Fu, *J. Phys. Chem. C* **2012**, *116*, 5764.
[106] H. Gülce, V. Eskizeybek, B. Haspulat, F. Sarı, A. Gülce, A. Avcı, *Ind. Eng. Chem. Res.* **2013**, *52*, 10924.
[107] Z. Pei, L. Ding, M. Lu, Z. Fan, S. Weng, J. Hu, P. Liu, *J. Phys. Chem. C* **2014**, *118*, 9570.
[108] B. Muktha, D. Mahanta, S. Patil, G. Madras, *J. Solid State Chem.* **2007**, *180*, 2986.
[109] D. Wang, J. Zhang, Q. Luo, X. Li, Y. Duan, J. An, *J. Hazard. Mater.* **2009**, *169*, 546.
[110] G. Liao, S. Chen, X. Quan, H. Chen, Y. Zhang, *Environ. Sci. Technol.* **2010**, *44*, 3481.
[111] Y. Zhu, Y. Dan, *Sol. Energy Mater. Sol. Cells* **2010**, *94*, 1658.
[112] H. Yan, Y. Huang, *Chem. Commun.* **2011**, *47*, 4168.
[113] S. Xu, L. Gu, K. Wu, H. Yang, Y. Song, L. Jiang, Y. Dan, *Sol. Energy Mater. Sol. Cells* **2012**, *96*, 286.
[114] J.-H. Huang, M. A. Ibrahem, C.-W. Chu, *RSC Adv.* **2013**, *3*, 26438.
[115] Y. Duan, Q. Luo, D. Wang, X. Li, J. An, Q. Liu, *Superlattices Microstruct.* **2014**, *67*, 61.
[116] D. Chowdhury, A. Paul, A. Chattopadhyay, *Langmuir* **2005**, *21*, 4123.
[117] D. Wang, Y. Wang, X. Li, Q. Luo, J. An, J. Yue, *Catal. Commun.* **2008**, *9*, 1162.
[118] S. Li, M. Chen, L. He, F. Xu, G. Zhao, *J. Mater. Res.* **2009**, *24*, 2547.
[119] Q. Li, C. Zhang, J. Li, *J. Alloys Compd.* **2011**, *509*, 1953.
[120] Q. Luo, X. Li, D. Wang, Y. Wang, J. An, *J. Mater Sci.* **2011**, *46*, 1646.
[121] B. Wang, C. Li, J. Pang, X. Qing, J. Zhai, Q. Li, *Appl. Surf. Sci.* **2012**, *258*, 9989.
[122] Y. Jia, P. Xiao, H. He, J. Yao, F. Liu, Z. Wang, Y. Li, *Appl. Surf. Sci.* **2012**, *258*, 6627.
[123] F. Deng, Y. Li, X. Luo, L. Yang, X. Tu, *Colloids Surf. A* **2012**, *395*, 183.
[124] S. Zhang, Q. Chen, Y. Wang, L. Guo, *Int. J. Hydrogen Energy* **2012**, *37*, 13030.
[125] Y. Yang, J. Wen, J. Wei, R. Xiong, J. Shi, C. Pan, *ACS Appl. Mater. Interfaces* **2013**, *5*, 6201.
[126] F. Duan, Q. Zhang, D. Shi, M. Chen, *Appl. Surf. Sci.* **2013**, *268*, 129.
[127] F. Li, E. Wang, X. Ni, *J. Mater Sci.-Mater. Electron.* **2013**, *24*, 5048.
[128] N. M. Dimitrijevic, S. Tepavcevic, Y. Liu, T. Rajh, S. C. Silver, D. M. Tiede, *J. Phys. Chem. C* **2013**, *117*, 15540.
[129] N. Sakai, G. K. Prasad, Y. Ebina, K. Takada, T. Sasaki, *Chem. Mater.* **2006**, *18*, 3596.
[130] T. Yang, H. Wang, X.-M. Ou, C.-S. Lee, X.-H. Zhang, *Adv. Mater.* **2012**, *24*, 6199.
[131] T. Bourgeteau, D. Tondelier, B. Geffroy, R. Brisse, C. Laberty-Robert, S. Campidelli, R. Bettignies, V. Artero, S. Palacin, B. Jousselme, *Energy Environ. Sci.* **2013**, *6*, 2706.
[132] X. Li, W. Lu, W. Dong, Q. Chen, D. Wu, W. Zhou, L. Chen, *Nanoscale* **2013**, *5*, 5257.
[133] T. Abdiryim, A. Ali, R. Jamal, Y. Osman, Y. Zhang, *Nanoscale Res. Lett.* **2014**, *9*, 89.
[134] R. Qiu, D. Zhang, Y. Mo, L. Song, E. Brewer, X. Huang, Y. Xiong, *J. Hazard. Mater.* **2008**, *156*, 80.
[135] O. P. Dimitriev, N. A. Ogurtsov, A. A. Pud, P. S. Smertenko, Yu. P. Piryatinski, Yu. V. Noskov, A. S. Kutsenko, G. S. Shapoval, *J. Phys. Chem. C* **2008**, *112*, 14745.
[136] F. Deng, L. Min, X. Luo, S. Wu, S. Luo, *Nanoscale* **2013**, *5*, 8703.
[137] W. Lee, R. S. Mane, S.-K. Min, T. H. Yoon, S.-H. Han, *Appl. Phys. Lett.* **2007**, *90*, 263503.
[138] Y. Han, C. Fan, G. Wu, H.-Z. Chen, M. Wang, *J. Phys. Chem. C* **2011**, *115*, 13438.
[139] Y.-G. Peng, J.-L. Ji, Y.-L. Zhang, H.-X. Wan, D.-J. Chen, *Environ. Prog. Sustain. Energy* **2013**, *33*, 123.
[140] Q. Luo, L. Bao, D. Wang, X. Li, J. An, *J. Phys. Chem. C* **2012**, *116*, 25806.
[141] H.-C. Liang, X.-Z. Li, *Appl. Catal. B: Environ.* **2009**, *86*, 8.
[142] Y. Zhu, S. Xu, D. Yi, *React. Funct. Polym.* **2010**, *70*, 282.
[143] S. Xu, Y. Zhu, L. Jiang, Y. Dan, *Water Air Soil Pollut.* **2010**, *213*, 151.
[144] F. Zhang, Y. Shi, Z. Zhao, W. Song, Y. Cheng, *Appl. Catal. B: Environ.* **2014**, *150–151*, 472.
[145] Y. Wang, M. Zhong, F. Chen, J. Yang, *Appl. Catal. B: Environ.* **2009**, *90*, 249.
[146] Y. Song, J. Zhang, H. Yang, S. Xu, L. Jiang, Y. Dan, *Appl. Surf. Sci.* **2014**, *292*, 978.
[147] D. Wang, L. Shi, Q. Luo, X. Li, J. An, *J. Mater. Sci.* **2012**, *47*, 2136.
[148] J. Krýsa, G. Waldner, H. Měšťánková, J. Jirkovský, G. Grabner, *Appl. Catal. B: Environ.* **2006**, *64*, 290.
[149] C. Sriwong, S. Wongnawa, O. Patarapaiboolchai, *Catal. Commun.* **2008**, *9*, 213.
[150] Q. Ding, Y.-E Miao, T. Liu, *ACS Appl. Mater. Interfaces* **2013**, *5*, 5617.
[151] M. E. Fabiyi, R. L. Skelton, *J. Photochem. Photobiol.* A **2000**, *132*, 121.
[152] W.-K. Jo, H.-J. Kang, *Ind. Eng. Chem. Res.* **2013**, *52*, 4475.
[153] J. S. Im, M. I. Kim, Y.-S. Lee, *Mater. Lett.* **2008**, *62*, 3652.
[154] A. R. Unnithan, N. A. M. Barakat, M. F. Abadir, A. Yousef, H. Y. Kim, *J. Mol. Catal. A: Chem.* **2012**, *363–364*, 186.
[155] C. Prahsarn, W. Klinsukhon, N. Roungpaisan, *Mater. Lett.* **2011**, *65*, 2498.
[156] A. Yousef, N. A. M. Barakat, S. S. Al-Deyab, R. Nirmala, B. Pant, H. Y. Kim, *Colloids Surf., A* **2012**, *401*, 8.
[157] H. Huang, X. Liu, J. Huang, *Mater. Res. Bull.* **2011**, *46*, 1814.
[158] J. Zeng, S. Liu, J. Cai, L. Zhang, *J. Phys. Chem. C* **2010**, *114*, 7806.
[159] R. Fateh, R. Dillert, D. Bahnemann, *ACS Appl. Mater. Interfaces* **2014**, *6*, 2270.
[160] R. M. Cámara, E. Crespo, R. Portela, S. Suárez, L. Bautista, F. Gutiérrez-Martín, B. Sánchez, *Catal. Today* **2014**, *230*, 145.

[161] S. Dadvar, H. Tavanai, H. Dadvar, M. Morshed, F. E. Ghodsi, *J. Sol-Gel Sci. Technol.* **2011**, *59*, 269.
[162] L. Rizzo, J. Koch, V. Belgiorno, M. A. Anderson, *Desalination* **2007**, *211*, 1.
[163] Y. Zhu, F. Piscitelli, G. G. Buonocore, M. Lavorgna, E. Amendola, L. Ambrosio, *ACS Appl. Mater. Interfaces* **2012**, *4*, 150.
[164] F. Kayaci, C. Ozgit-Akgun, I. Donmez, N. Biyikli, T. Uyar, *ACS Appl. Mater. Interfaces* **2012**, *4*, 6185.
[165] F. Kayaci, C. Ozgit-Akgun, N. Biyikli, T. Uyar, *RSC Adv.* **2013**, *3*, 6817.
[166] C.-S. Lee, J. Kim, J. Y. Son, W. Choi, H. Kim, *Appl. Catal. B: Environ.* **2009**, *91*, 628.
[167] M. Sökmen, İ. Tatlıdil, C. Breen, F. Clegg, C. K. Buruk, T. Sivlim, Ş. Akkan, *J. Hazard. Mater.* **2011**, *187*, 199.
[168] T. Sivlim, Ş. Akkan, İ. Altın, M. Koç, M. Sökmen, *Water Air Soil Pollut.* **2012**, *223*, 3955.
[169] H. Han, R. Bai, *Ind. Eng. Chem. Res.* **2009**, *48*, 2891.
[170] H. J. Kim, H. R. Pant, A. Amarjargal, C. S. Kim, *Colloids Surf., A* **2013**, *434*, 49.
[171] T. J. Athauda, U. Butt, R. R. Ozer, *RSC Adv.* **2013**, *3*, 21431.
[172] Z. Chang, *Chem. Commun.* **2011**, *47*, 4427.
[173] C. Su, Y. Tong, M. Zhang, Y. Zhang, C. Shao, *RSC Adv.* **2013**, *3*, 7503.
[174] S. Ye, D. Zhang, H. Liu, J. Zhou, *J. Appl. Polym. Sci.* **2011**, *121*, 1757.
[175] H. Kong, J. Song, J. Jang, *Environ. Sci. Technol.* **2010**, *44*, 5672.
[176] R. Y. Hong, J. H. Li, L. L. Chen, D. Q. Liu, H. Z. Li, Y. Zheng, J. Ding, *Powder Technol.* **2009**, *189*, 426.
[177] H. Yu, Q. Dong, Z. Jiao, T. Wang, J. Ma, G. Lu, Y. Bi, *J. Mater. Chem. A* **2014**, *2*, 1668.
[178] B. Pan, Y. Xie, S. Zhang, L. Lv, W. Zhang, *ACS Appl. Mater. Interfaces* **2012**, *4*, 3938.
[179] Y. Xie, L. Lv, S. Zhang, B. Pan, X. Wang, Q. Chen, W. Zhang, Q. Zhang, *Nanotechnology* **2011**, *22*, 305707.
[180] Y. Xie, S. Zhang, B. Pan, L. Lv, W. Zhang, *Chem. Eng. J.* **2011**, *174*, 351.
[181] J. V. Antony, P. Kurian, N. P. N. Vadakkedathu, G. E. Kochimoolayil, *Ind. Eng. Chem. Res.* **2014**, *53*, 2261.
[182] C. Sriwong, S. Wongnawa, O. Patarapaiboolchai, *J. Environ. Sci.* **2012**, *24*, 464.
[183] F. Magalhães, R. M. Lago, *Sol. Energy* **2009**, *83*, 1521.
[184] L. Zhang, L. Yin, C. Wang, N. Lun, Y. Qi, *ACS Appl. Mater. Interfaces* **2010**, *2*, 1769.
[185] Y. Li, W. Xie, X. Hu, G. Shen, X. Zhou, Y. Xiang, X. Zhao, P. Fang, *Langmuir* **2010**, *26*, 591.
[186] F. Lu, W. Cai, Y. Zhang, *Adv. Funct. Mater.* **2008**, *18*, 1047.

Received: May 28, 2014
Revised: June 24, 2014
Published online: July 29, 2014

